Available online at www.sciencedirect.com

SCIENCE DIRECT®

Journal of Applied Geophysics 58 (2006) 330–350

JOURNAL OF APPLIED GEOPHYSICS

www.elsevier.com/locate/jappgeo

Theory of EM monitoring of sea bottom geothermal areas

Sergey Ershov [a], Irina Mikhaylovskaya [b], Oleg Novik [c,*]

[a] *Keldysh Inst. for Appl. Math. of Russian Acad. Sci., Moscow, 125047, Russia*
[b] *Moscow State University, Faculty for Math., Moscow, 119899, Russia*
[c] *Institute of Terrestrial Magnetism, Ionosphere and Radio Wave Propagation of RAS, 117246, POB 51, Moscow, Russia*

Received 8 December 2003; accepted 31 May 2005

Abstract

Monitoring of geophysical conditions of marine sedimentary basins is necessary for predicting seismic events and for adaptation of geothermal technologies for seismically active (as a rule) sea bottom geothermal areas. These conditions are characterized by seismo-hydro-electromagnetic (EM) geophysical field interaction in the presence of gravity. Based on the main physical principles, geophysical and petrophysical data, we formulate a mathematical model of seismo-hydro-EM interaction in a basin of a marginal sea and calculate the transformation of a seismic excitation in the upper mantle under the central part of the sea of Japan into the low-frequency (0.1 to 10 Hz) EM signals at the top of the sea bottom sedimentary layer, at the sea surface and in the atmosphere up to the lower boundary of the ionosphere. Physics of the EM generation and propagation process is shown including: generation of EM waves in the upper mantle layer M by a seismic wave from under M, spatial modulation of diffusive EM waves by a seismic wave, stopping of the EM wave arrived (before the seismic P wave) from the upper mantle at the top of the sediments because of the high electric conductivity of seawater (3.5 S/m), immediate penetration of the EM wave through the seawater thickness after the delayed seismic P wave shock into the sea bottom, and EM emission from the sea surface into the atmosphere. Let us note that the EM signal in the sea bottom sediments is the first measurable signal of a seismic activation of geological structures beneath the seafloor and this signal is protected by seawater from the influence ionosphere disturbances. Amplitude of the computed magnetic signals (300, 200, 50, and 30 pT at the ocean–atmosphere interface and at the height of 10, 30 and 50 km, respectively), their predominant frequency (0.25 Hz), the delay of the seismic P wave in regard to the magnetic signal for the receivers at the shore (20 s), the amplitude of temperature disturbances in sediments (up to 0.02 K), the parameters of the long (150 km) tsunami wave of a small (up to 20 cm) amplitude far from the shore and other values that characterize the seismo-hydro-EM process are of the orders observed. Recommendations for the EM monitoring of dynamic processes beneath seafloor geothermal areas are given.

Keywords: Sea bottom; Geothermal areas; Earthquake monitoring; Mathematical models

* Corresponding author. Tel.: +7 95 332 2808; fax: +7 95 7274881.
E-mail address: onovik@online.ru (O. Novik).

0926-9851/$ - see front matter © 2005 Elsevier B.V. All rights reserved.
doi:10.1016/j.jappgeo.2005.05.009

1. Introduction

Sea bottom areas with a heightened heat flow are located mostly in tectonically active regions of the Ocean (covering about 75% of the Earth surface) as well as continental geothermal areas.

Geographic correlation between lithosphere zones with high seismic activity and ones with high geothermal activity (and high electric conductivity) is well-known. It is supposed (in the theory of metallogeny) that fragmentation of geological structures caused by an intensive tectonic regime supplies plenty of channels for the transfer of heat and mass (metals and other chemicals dissolved in high temperature fluids) from the asthenosphere into the upper stages of the lithosphere. For example, the Sea of Japan, a marginal sea in the tectonically active Pacific segment, is characterized by a rather high heat flow (up to 4 HFU) through its bottom. The geothermal technology may be regarded as a power and raw material technology with renewal sources and without emission of greenhouse gases. This technology may not be adapted to sea bottom geothermal areas while dynamical processes in ocean geological structures are being ignored.

Is it possible to apply electromagnetic (EM) measurements for monitoring seismic processes beneath a seafloor? This is the main problem we are trying to investigate in this paper on the basis of physical principles, mathematical methods and geophysical data. This problem is closely connected with the general marine geophysical research, sea bottom observations and technology (McDuff, 1995; Novik and Mikhaylovskaya, 1998; Novik et al., 1998, 2000b; Romanowicz et al., 2001).

EM signals associated with seismic activity of oceanic lithosphere have been detected more than once, in particular in near sea Pacific regions. The lithosphere–ionosphere EM coupling is being widely investigated as well, especially in view of EM signals recorded by satellites' instrumentation above the earthquake preparation zones (Belov et al., 1974; Biagi et al., 1998; Hayakawa and Molchanov, 2002; Johnston, 1997; Johnston and Parrot, 1998; Iyemori et al., 1996; Shpakovsky et al., 2002).

But the physical mechanism of these seismo-EM phenomena is not well understood (and the words 'associated with seismic activity' are used by the researches instead of 'caused by seismic activity'). The relation between characteristics of EM signals in the atmosphere, on the one hand, and characteristics of seismic excitations of the oceanic lithosphere and tsunami waves, on the other hand, especially at a quantitative level needed for monitoring and prognosis, is also not yet clear.

We believe that the relation between EM signals and seismic excitation is being formed during the process of the generation of EM disturbances in the neighborhood of an earthquake hypocenter and their propagation along a lithosphere-hydrosphere-atmosphere path. In its turn, this generation and propagation process is a result of seismo-hydro-EM geophysical field interaction and transformation in the lithosphere–hydrosphere–atmosphere system. Thus, to investigate the relation between EM signals and seismic excitation, we must formulate a mathematical model of seismo-hydro-EM interaction (see Section 2 and the Appendix), trace numerically the signal generation and propagation as a field transformation process (Section 3, Figs. 3–10) and then consider (Section 4, Figs. 11–14) the time series of the signals. In Section 5 we discuss: the accuracy of the algorithm, correspondence between numerical results and measurements, and necessity to develop the theory and practice of monitoring of geophysical conditions of sea bottom geothermal areas in parallel with technological and economical investigations.

Results of this paper have been discussed at the General Assembly of the EGS-2000, Fall-2000 meeting of the AGU, and other meetings; short English versions of these reports may be found in (Ershov et al., 2001; Novik et al., 2000a,b, 2001). Transformation of elastic displacements in the upper mantle under the sea into EM signals at its surface and above is computed here on the basis of the magneto-thermo-elasticity and "shallow water" theories (Maugin, 1988; Stoker, 1957) combined together; the physical approach, mathematical methods and algorithms were developed in (Novik, 1995; Novik and Ershov, 2001).

We compute EM signals propagating ahead of a seismic wave caused by the model seismic excitation, i.e. we consider co-seismic signals, but the term 'seismic' (or 'seismo-') is used instead of 'co-seismic' everywhere, save for Section 5.

2. Model medium and its seismic excitation

The model medium includes a lithosphere domain up to the earth's upper mantle, sea, and the atmosphere domain up to the lower boundary of the ionosphere. The model lithosphere domain and the sea are shown in Fig. 1. The cross-section runs from the Bay of Peter the Great throughout the Pervenets Rise, the Yamato Basin, and ends at the North Yamato Rise. The co-ordinates $x=(x,y)$ are chosen so that the vertical axis is directed *downwards* with the vertical co-ordinate $x=0$ being the sea surface, and y is the horizontal co-ordinate increasing from left to right. The third coordinate z is normal to the cross-section plane. According to the chosen direction of the vertical co-ordinate axis, $x>0$ in the sea and in the lithosphere and $x<0$ in the atmosphere. In most computations, the upper boundary of the model domain is $x=L_D=-70$ km.

The characteristics of the sedimentary (S), granite metamorphic (G) and basalt (B) layers (basalt layer overlays the higher electrically conductive upper mantle layer M and the 2D geometry is applied) are usual from the petrophysical viewpoint (Hellweg, 1982) and may be regarded as approximately similar to the characteristics of the mentioned cross-section of the central part of the Sea of Japan. The values (in SI units) of density ρ, elastic wave velocities v_p and v_s, electric and thermal conductivities σ_e and κ, and density of the power of heat sources q are shown in Table 1. Everywhere the heat capacity is $c_V=1$ [kJ/(kg × K)] and the magnetic permeability is $\mu_e=\mu_0=4\pi\times10^{-7}$ (SI units), i.e. the value for vacuum.

Table 1
Physical parameters of the medium

	ρ, kg/m^3	v_p, m/s	v_s, m/s	σ_e, S/m	κ, W/(m × K)	q, μW/m^3
W	1000	–	–	3.5	–	–
S	2500	5000	3000	0.005	1.3	1.2
G	2700	5800	3200	0.001	2.5	0.9
B	2900	6300	4000	0.005	2.1	0.4
M	3300	7200	4800	0.020	3.2	0.4

The higher conductivity of M reflects the well-known distinctive geographic correlation between high-conductivity and high-seismicity lithosphere zones (e.g., Arora and Mahashabde, 1987; Bragin et al., 1993; Honkura, 1974; see the Introduction). We suppose that the medium is isotropic and its physical characteristics are stationary and spatially continuous due to existence of the thin transitional layers between the main ones shown in Table 1 and Fig. 1, including the transition from S to W. Polarization and thermoelectric effects in rocks

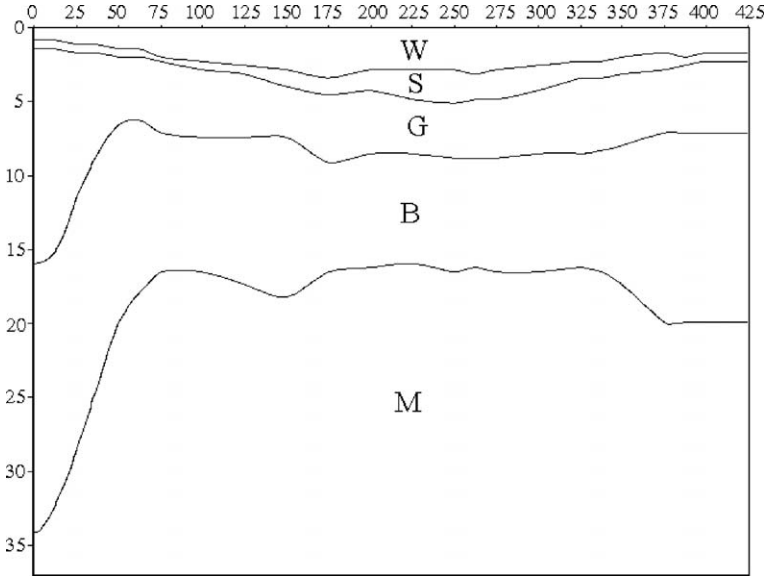

Fig. 1. The sea (W, water) and the geological structure of the lithosphere part of the medium: S — sediments, G — granitoids, B — basalts, M — the upper mantle, depths under the sea level (0) and horizontal co-ordinates are in km. The cross-section end-points are: (43.2 °N, 132 °E) and (39.7 °N, 133.7 °E).

and electric conductivity of atmosphere above the sea are neglected.

We shall assume that there are no insulators in the lithosphere part and frequencies of all processes are low enough, so displacement currents are negligible in comparison with conductivity ones. We deal with electromagnetic (EM) signals of a tsunami on the stage of a long hydrodynamic wave of a small amplitude far from a coast, and use the non-linear equations of the "shallow water" theory.

Now let us come to the seismic excitation of the model medium. The vector $u_0=(u_{01},u_{02})$ describes the elastic displacements at the low boundary $x=L_1=37$ km of the lithosphere part of the model medium (Fig. 1) arising due to the seismic wave arriving at this boundary from a deeper source. Here and below subscripts *1* and *2* denote vertical and horizontal components of a vector value.

The duration of this excitation (varied in different simulations) is several seconds, the amplitude is about 5 cm, the predominant frequency is 0.25 Hz, and the excitation decays with time and with the distance from the center of the domain (Fig. 2):

$$u_{01} = a_1 \times te^{-bt-\alpha(y-y_0)^2}\cos(\omega t)\cos\frac{2\pi y}{d} \equiv A(y)f(t),$$

$$u_{02} = a_2 \times te^{-bt-\alpha(y-y_0)^2}\sin(\omega t)\sin\frac{2\pi y}{d} \equiv 0.5A(y)f(t)$$

where $a_1=7$ cm, $a_2=3.5$ cm, $b=1/3\ \mathrm{s}^{-1}$, $\alpha=5\times10^{-11}$ m^{-2}, $\omega=5/3$ Hz, $y_0=L_2/2=212.5$ km, $d=150$ km. So, the main component of the seismic excitation is vertical in this example of the input data.

Our simulation algorithms allows us to compute the evolution of fields under a wide class of initial and boundary conditions, including volume seismic excitation instead of a boundary excitation. We have used other acceptable values of the physical parameters in Table 1 and other characteristics of the excitation as well as different (but mathematically correct) conditions at the outer boundaries $x=L_1$, $x=-L_D$ and $y=0$, $y=L_2$.

Besides, we varied the boundaries of the lithosphere layers. But the evolution of the model seismic perturbations of the fields, especially the relation between seismic excitations under the sea bottom and EM signals at the sea surface and above were quite similar to those described in Section 3.

The system of the partial differential equations of the seismo-hydro-EM geophysical fields' transformation resulting in seismo-EM signals above the sea under the assumptions of this Section on the medium and processes is formulated in the Appendix (the non-principal assumptions are formulated there). These equations, the initial, boundary and contact conditions, and characteristics of the medium and seismic excitation form the mathematical model we use in the next Section.

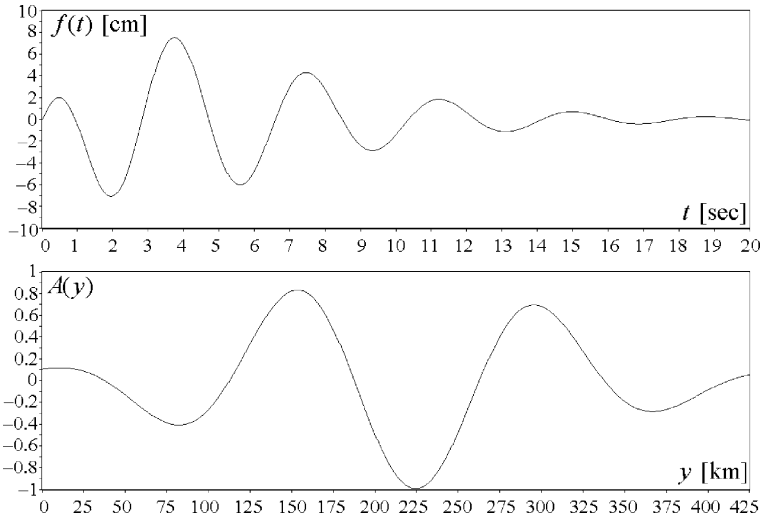

Fig. 2. The temporal $f(t)$ and spatial $A(y)$ modulation of the vertical component $u_1(t,y)$ of elastic displacements in the upper mantle beneath the sea floor (seismic excitation); the horizontal component $u_2(t,y)$ is approximately the same save the amplitude which is half as many as the one of $u_1(t,y)$.

3. Seismo-hydro-EM geophysical fields' transformation

In this Section we describe the sequential stages of the transformation (Figs. 3–10) of a seismic excitation (elastic displacements are considered here, see Fig. 2) in the upper mantle layer beneath the seafloor into EM signals in the atmosphere above the sea (Section 4).

The lithosphere EM signal arises at the bottom of the conductive upper mantle layer M (see Fig. 1 and Table 1), where the seismic excitation, determined in the previous Section, is supposed to be localized at the moment $t=0$, and reaches the depth $x=25$ km by the moment $t=1$ s with the amplitude of about 20 pT. Because of the higher conductivity of M this initial seismo-EM generation and propagation is similar to the case of a low resistivity block deformed by a seismic wave in the presence of geomagnetic field (Novik et al., 1998).

The seismo-hydro-EM interaction at the moment $t=2.50$ s after the beginning of the seismic excitation beneath the sea floor is shown in Fig. 3. In every panel, the horizontal co-ordinate y [km] is shown above the upper horizontal boundary. The vertical coordinate x [km] is shown at the left boundary, $x=0$ is the sea surface. The time t [s] after the beginning of the seismic pulse and maximal and minimal field values see at the right boundary of every panel.

We shall use the following definition of the "front" of a scalar diffusive signal at the moment t: it is the curve where a field value under consideration (e.g. modulus of one of the components) crosses at the moment t the sensitivity threshold of measurements. For the diffusive B_2 signal propagating upward (our

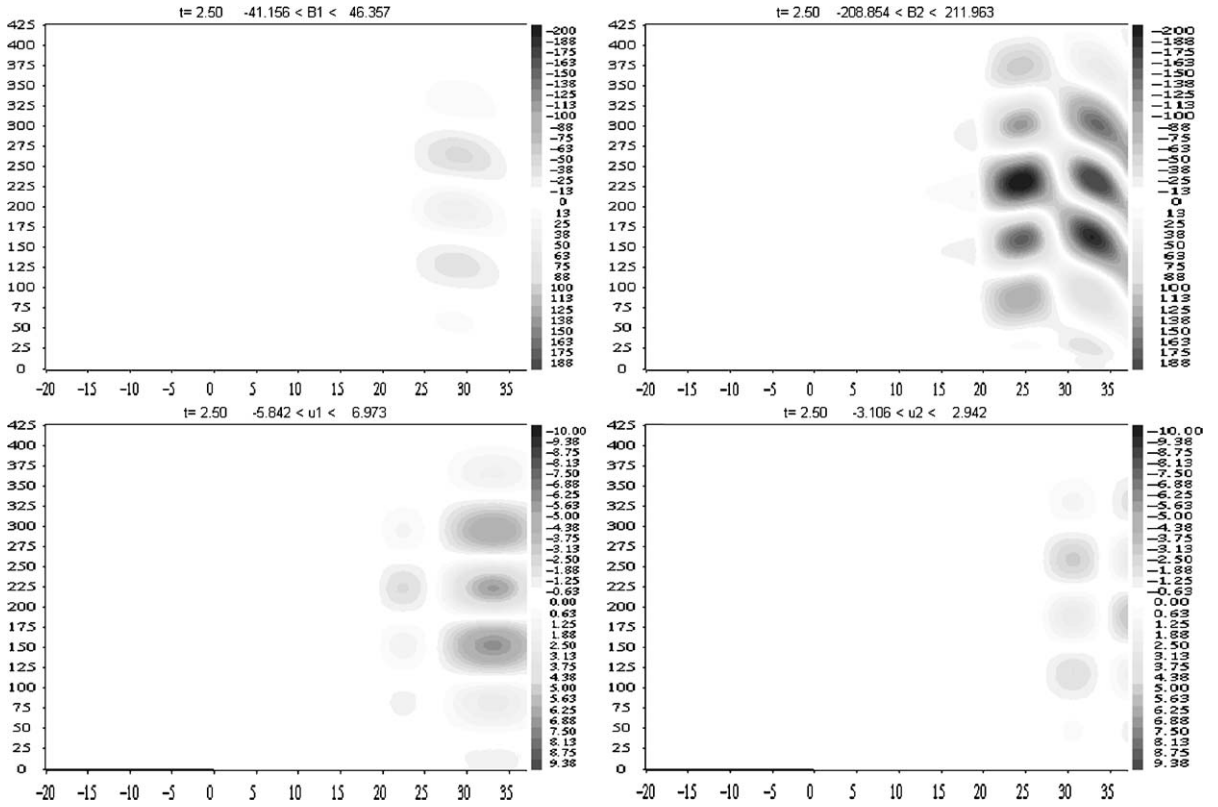

Fig. 3. The horizontal component B_2 [pT] of the seismic disturbance of the magnetic field entered from upper mantle to the crust (the lower right panel, the vertical component B_1 is shown at the upper right panel); the fields of vertical (u_1 [cm]) and horizontal elastic displacements are located in the upper mantle yet, $t=2.50$ s after the beginning of seismic excitation; beneath is the gray scale legend in interval −200 to 200 pT.

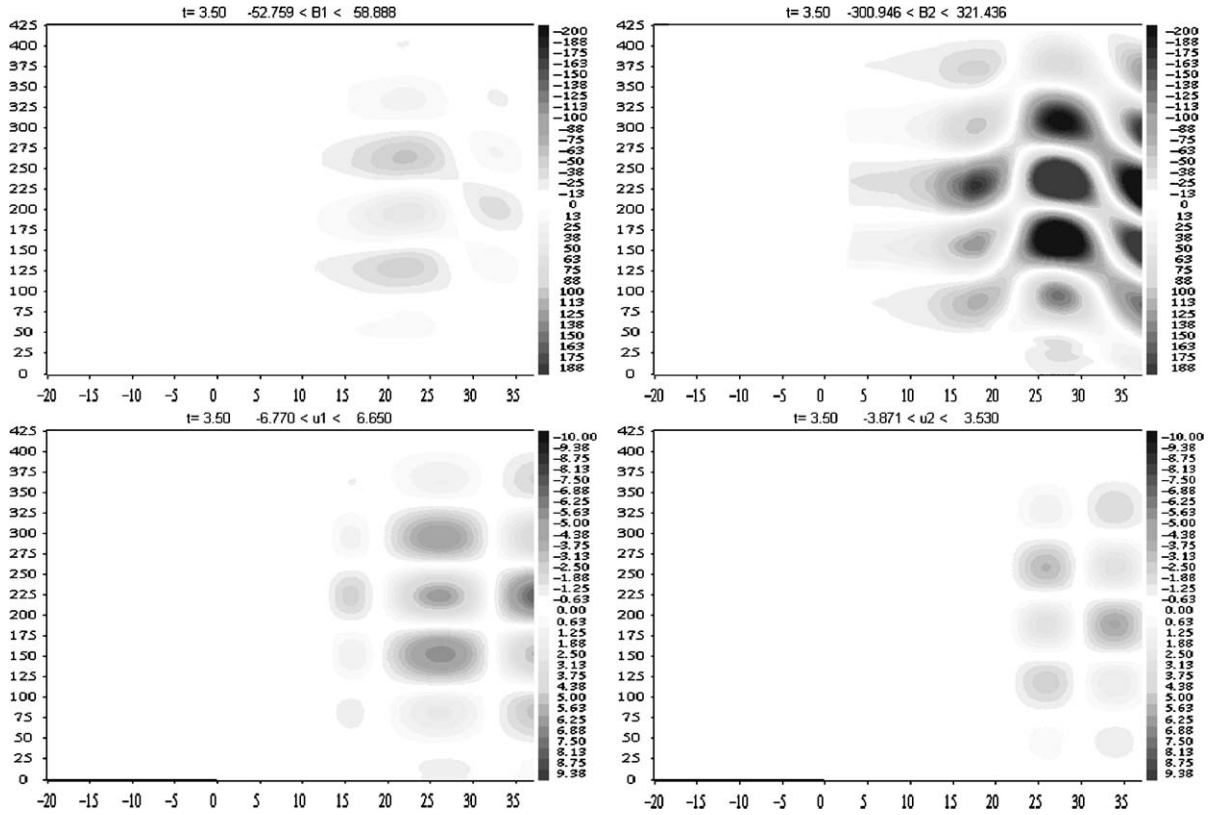

Fig. 4. The magnetic disturbance component B_2 [pT] arrived (t=3.50 s) at the sea bottom's surface; B_1, S and P waves delayed. The spatial structure of B_2 is similar to one of the seismic P-wave u_1 (*spatial seismic modulation of an EM wave*).

case) the signal above the "front" is weaker than the sensitivity threshold whereas the signal under the "front" is stronger than the threshold. In visualization, when field amplitude is color-coded, the sensitivity is replaced by resolution of color fringes (the gray scale is used in this paper). Rather weak signals (<5 pT) are invisible in our visualization (similarly to a noise signal discrimination by field measurements), i.e. the area with that level of the field remains white. Gray scale is shown under the low boundary of every panel and corresponding units are used: cm for the components of mechanical displacements (left panels) and pT for the components of the magnetic field. The gray color of the same intensity is used to imagine positive and negative field values with the same modulus. So the sign at the scale under every panel may be neglected. In other words, only modulus of the field components are imaged, because different colors are not used in this paper.

In Fig. 3, the horizontal component B_2 [pT] of the magnetic field disturbance entered from the upper mantle to the crust (lower right panel, the "front" of B_2 is at the depth of 20 km under the sea level); the fields u_1 [cm] of vertical elastic displacements (i.e. the seismic P-wave, the upper left panel) and u_2 (S-wave) of horizontal displacements are located in the upper mantle yet.

The magnetic induction component B_2 is a diffusive field (the displacement current is negligible, see the previous Section) represented locally by oscillations of rather low main frequencies from 0.1 to 10 Hz (e.g. Fig. 11). Nevertheless, B_2 is spatially periodic and the spatial period is not compatible with these frequencies. As a matter of fact, B_2 approximately "inherits" the periodic structure of the seismic wave (cf. the upper left and the low right panels of Fig. 3 and see Fig. 2). We can consider this phenomenon as a *spatial seismic modulation of an ULF diffusive electromagnetic field*. This

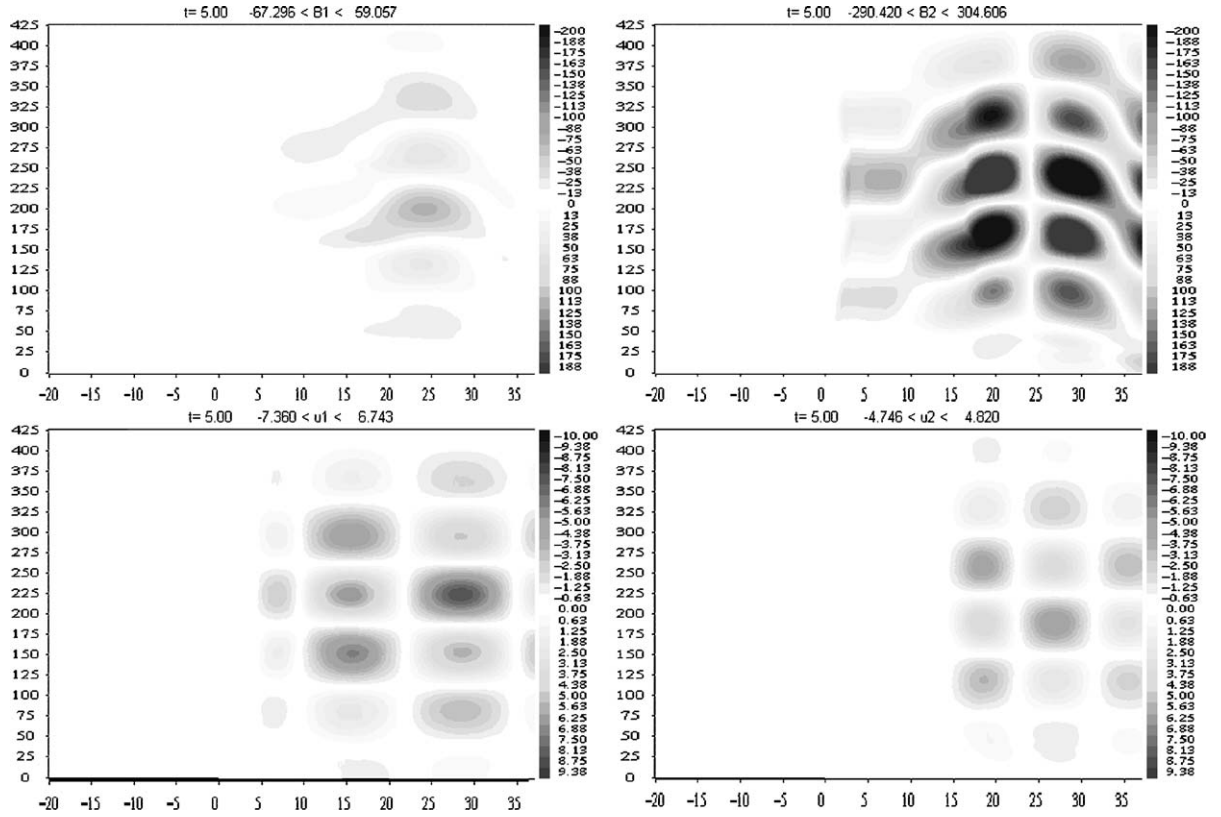

Fig. 5. The seismo-hydro-EM interaction at the moment $t=5.00$ s: the change of the spatial structure of the horizontal magnetic induction B_2 is negligible as compared with one at the moment $t=3.50$ s (a "*frozen*" *magnetic field* caused by a high sea water electric conductivity).

modulation appears distinctively by diffraction of a seismic wave by a low-resistivity (0.1 S/m) block typical for seismically active lithosphere zones (Novik et al., 1998).

Now let us come to the next stage and correspondingly to other features of the model seismo-hydro-EM tsunami process.

In the crustal layers B, G, and S, which have lower electric conductivity in comparison with layer M, see Table 1, the propagation of the EM signal accelerates and *reaches the sea bottom with an amplitude of 50 pT* for the horizontal magnetic component B_2 at the moment $t=3.50$ s (low right panel of Fig. 4); the vertical magnetic component B_1 (upper right panel) is delayed in regard to B_2 as well as P and S seismic waves (left panels of Fig. 4). This signal is the first *distinctive* (and protected by the sea water from ionosphere EM disturbances) magnetic signal caused by the seismic excitation. It is seen from Fig. 4 that it remains spatially modulated by the seismic wave.

During the next stage of the computed seismo-hydro-EM process, propagation of the lithosphere EM signal significantly decelerates due to the high electric conductivity (3.5 S/m, Table 1) of the sea water: in the interval $3.50 \le t \le 5.30$ s, i.e. before the arrival of the seismic P wave at the sea bottom, the configuration of the seismic magnetic field component B_2 looks "*frozen*" (Figs. 4 and 5, low right panels). In particular, its "front" (above) is replicating approximately the sea bottom surface during this time interval. It is seen from Figs. 3–5 that in an isotropic medium the vertical seismic magnetic field component B_1 (the one parallel to the main component of the seismic excitation, see previous Section) is propagating rather differently as compared with B_2. Indeed, the seismic modulation of B_1 is absent, B_1 is delayed in regard to B_2, and B_1 is not "frozen" because the surface of the sea bottom was not achieved by B_1 at the moment $t=5$ s (other distinctions shall be described below). Let us note that a similar dependence of the peculiarities of the

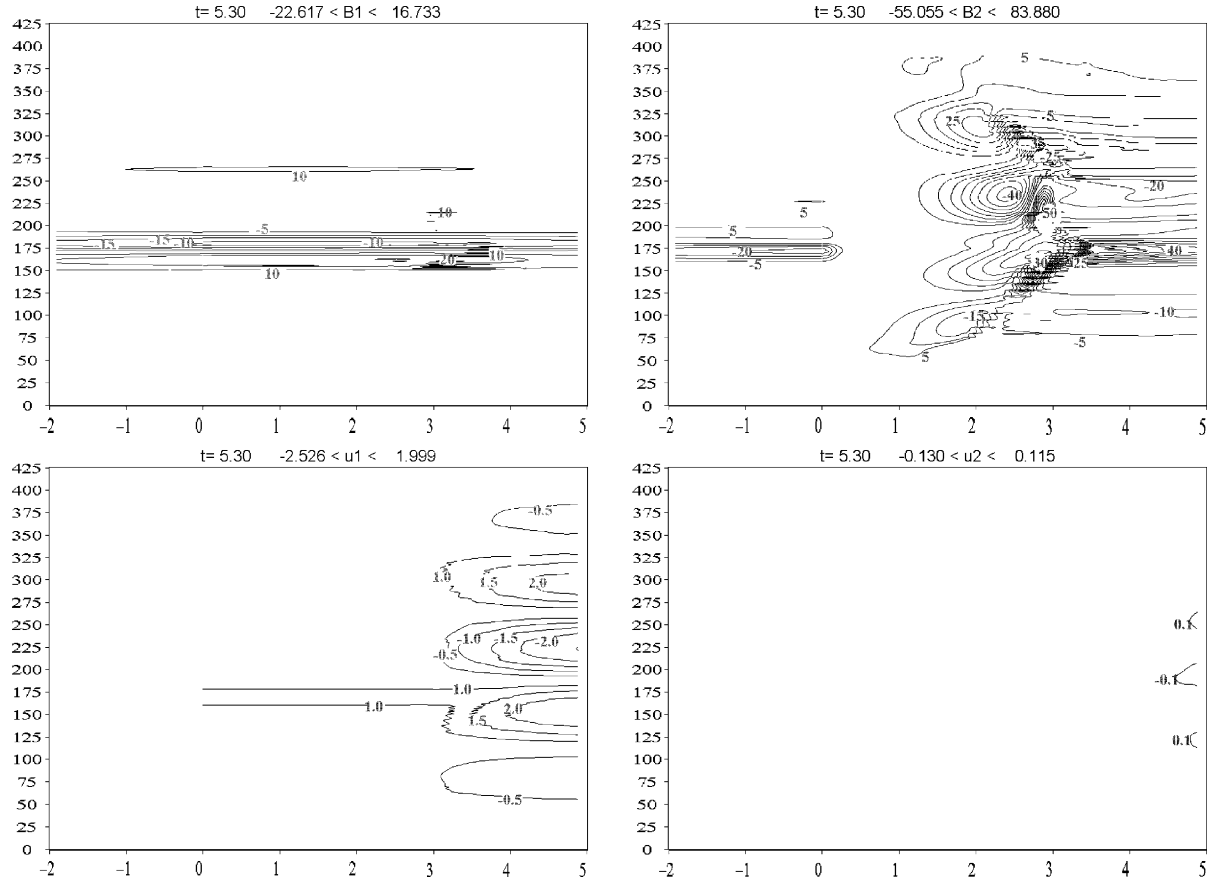

Fig. 6. *The seismic P-wave shock into the sea bottom generates a column of a vertical flow* above the P-wave front contact with the sea bottom's surface (the upper left panel); *the domain of negligible (<5 pT) values (the "spatial rupture") of horizontal component of magnetic induction* caused by the shock (the lower right panel); the vertical magnetic component B_1 [pT] is generated in the sea without the domain of the "rupture" (the upper right panel); the S-wave does not affect the hydrodynamic field at this moment (the lower left panel), $t=5.30$ s.

propagation of different components of a seismic magnetic disturbance (in isotropic media) on polarization of a seismic excitation had been observed by simulation of seismo-EM interaction in a model continental lithosphere zone with a low-resistivity block (Novik et al., 1998).

The next stage after the EM field "freezing" is the *shock of the seismic P wave into the sea floor* at the moment $t_p=5.3$ s *and EM emission from the sea surface into the atmosphere*. To consider in detail the computed seismo-hydro-EM interaction at this main stage, we use contour plots of the fields and extract a narrow zone with height of 2 km above the sea level and depth of 5 km: the vertical co-ordinate x [km] is shown at the left boundary of every panel of Fig. 6 ($-2\le x\le 5$), $x=0$ corresponds to the sea surface; $0\le y\le 425$ [km], the lower and upper bounds of the field values in the considered medium are shown at the right boundaries of the panels. The upper left panel of Fig. 6 presents contour plot of the field of vertical displacements u_1 [cm] in the crust and in the sea; the lower left panel presents horizontal elastic displacements u_2 [cm] in the crust near the sea bottom; as usually, the magnetic field is shown in the right panels. Contour lines are numbered by magnetic induction values (beginning from ± 5 pT) for the right panels and by displacement values (from ± 0.1 cm) for the left panels (namely, elastic displacements beneath the seafloor and hydrodynamic ones in the sea).

One can see (Fig. 6) that the seismic P-wave of vertical displacements caused a column, say $Q(t)$, of a vertical flow above the area of the P wave front

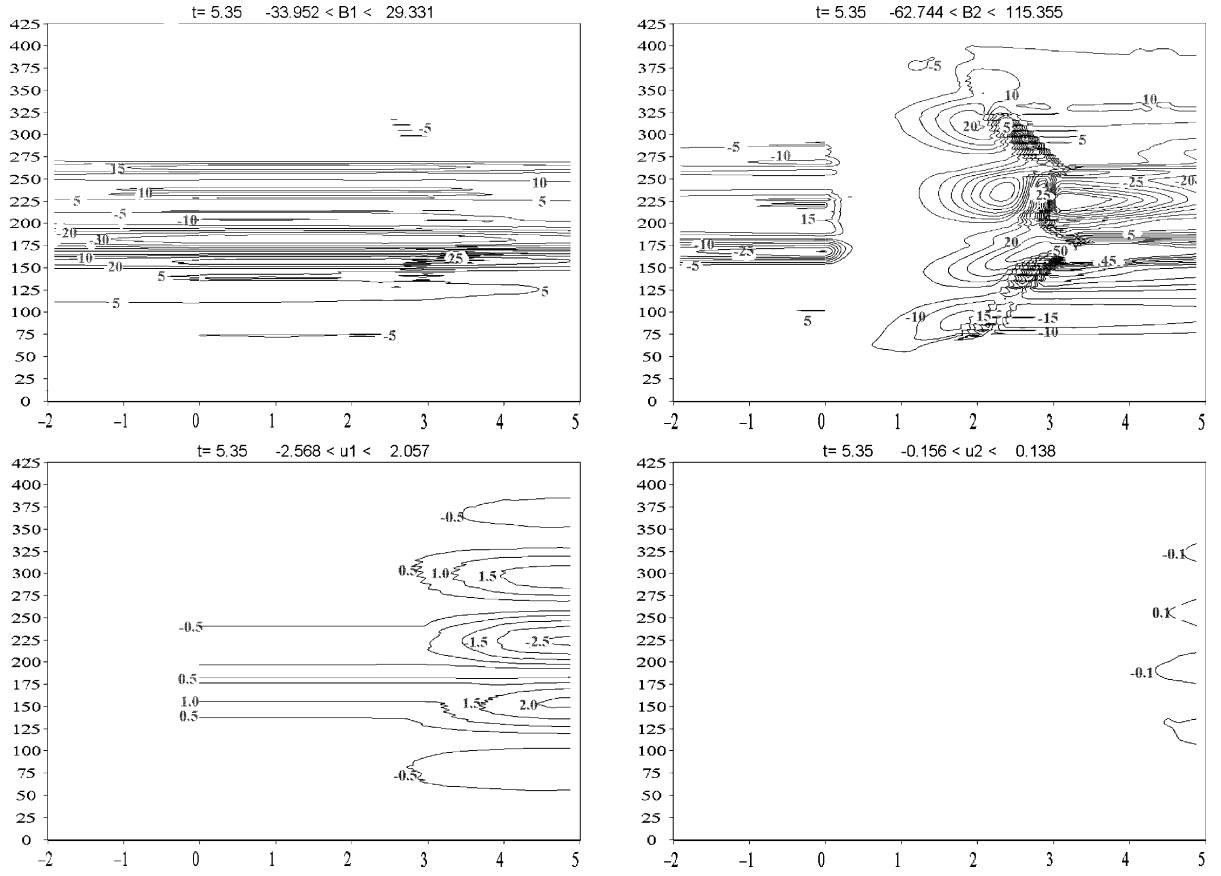

Fig. 7. Spreading of the seismo-hydrodynamic (upper left panel) disturbance and the seismic magnetic signal (the upper right panel); *beginning of diffusion of the horizontal magnetic component generated near the sea surface into the sea depth* (the lower right panel), $t=5.35$ s.

contact with the sea bottom surface and the magnetic field in the sea is generated in the moving sea water part $Q(t)$. The contour plot of the horizontal magnetic field component B_2 [pT] (the lower right panel) shows a domain of negligible ($|B_2|<5$ pT) field values (a "spatial rupture") whereas the vertical component B_1 [pT] is generated in $Q(t)$ without similar spatial peculiarities (the upper right panel). The S-wave does not affect the hydrodynamic field at this moment (the lower left panel).

After the moment $t=t_p=5.3$ s the perturbation of the magnetic field is spreading in the sea water and atmosphere, the magnetic component B_2 diffusing from the sea surface and through the seafloor *inside* the sea interior, and, as a result, the rupture of magnetic field is attenuating (Fig. 7, $t=5.35$ s and Fig. 8, $t=5.50$ s) and the seismo-hydrodynamic (i.e. generated in the sea water) horizontal magnetic component B_2 is joining with B_2 penetrating into the sea from the lithosphere (Fig. 9, $t=6.05$ s). The rupture disappears about 10 s after the beginning of the seismic excitation in the upper mantle layer M.

In Fig. 10, the fields are shown at time $t=15$ s. The surface of the sea bottom is seen distinctively at the lower right panel representing the horizontal component of the seismo-hydro-magnetic signal (i.e. a magnetic signal resulting from seismo-hydro-EM interaction in the considered lithosphere–hydrosphere–atmosphere model medium). The sea is filled with EM energy (right panels) and with seismic P wave energy (upper left panel); the S wave is not penetrating into the sea practically (lower left panel) because the sea bottom surface is approximately flat and the tangent stress is supposed to be zero according to the elasto-hydrodynamic contact conditions (Appendix, Eqs. (A.1)–(A.5)). The seismo-hydro-magnetic signal

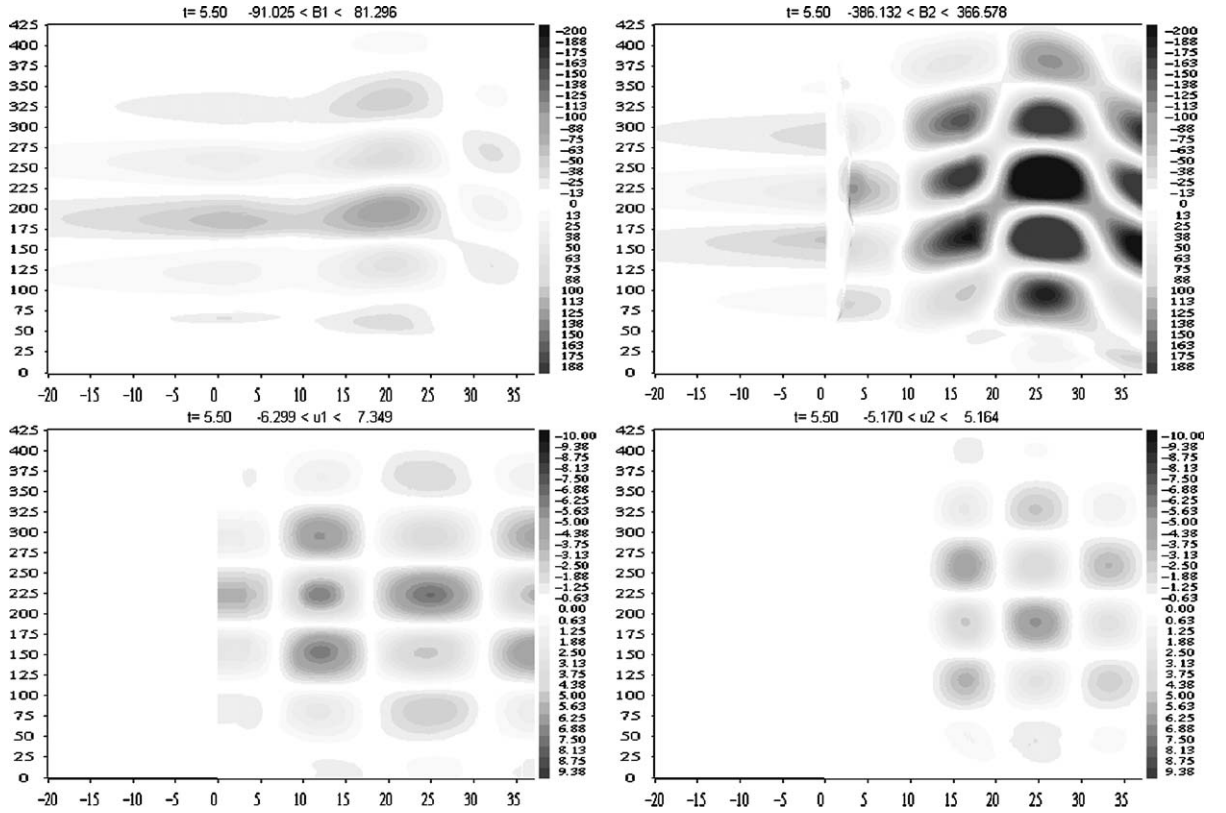

Fig. 8. The spatial structure of the horizontal (B_2 [pT], the lower right panel) and vertical (B_1, the upper right panel) components of magnetic induction in the sea, $t=5.50$ s i.e. 0.2 s after the seismic P-wave u_1 [cm] arrival at the sea floor (the upper left panel); the seismic S-wave (u_2, the lower left panel) delays in regard to the P-wave, the "*spatial rupture*" *is reducing*.

above the sea is considerably non-homogeneous in the horizontal co-ordinate and its peaks correspond to the structure of the seismic magnetic field under the sea bottom which, in its turn, is spatially modulated (lower right panel) by seismic P wave (upper left panel of Fig. 10).

4. Seismo-em signals above the sea

In the previous Section we described the evolution of the spatial structure of fields included in seismo-hydro-EM interaction process. According to the physical mechanism investigated, we show here the evolution of the seismic magnetic field disturbances, i.e. seismic magnetic signal time series, in fixed points at the sea–air interface and above caused by the model seismic excitation determined in Section 2.

These seismic EM signals at the sea surface (Figs. 11 and 14) and above (Figs. 12 and 13) are oscillations of the same low frequency range 0.1 to 10 Hz as the seismic excitation in the upper mantle (Fig. 2). According to the assumption about incompressibility of the sea water and neglect of the air conductivity, these signals arise at the moment $t_p=5.3$ s of the seismic P wave's arrival at the sea bottom surface. At the sea–atmosphere interface ($x=0$) the signal amplitude is a few hundreds of pT for the vertical (B_1) and horizontal (B_2) components of the magnetic induction at the point with horizontal co-ordinate $y=200$ km. Figs. 12 and 13 show the attenuation of seismic ultra-low frequency EM signals at the heights of 10 and 50 km above the sea surface up to a few tens of pT near the low boundary of the ionosphere domain D. Let us note that the seismic magnetic signal's amplitude

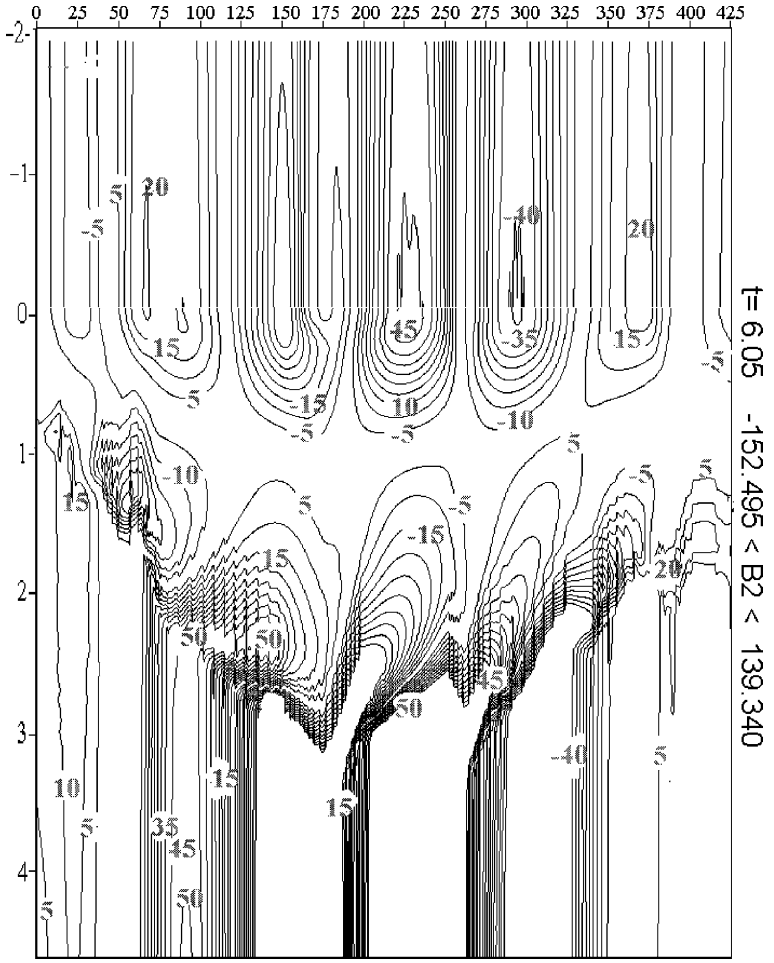

Fig. 9. *Joining* of the lithosphere part of the horizontal component of the seismic magnetic disturbance with the seismo-hydrodynamic part of this disturbance (seismic magnetic field contours reconnection), $t=6.05$ s.

for the horizontal (B_2) and vertical (B_1) component is about 100 pT at the sea surface by $y=100$ km (Fig. 14), i.e. at the distance of 100 km from the 1st point, in other words the signal attenuation along the sea surface is not so fast as at heights above the sea (Figs. 11–13).

As a matter of fact according to our approach, an ultra-low frequency magnetic signal accompanying the seismo-hydrodynamic wave may be measured by usual devices whereas the amplitude of this long (about 150 km) wave far from the shore is too small to be discovered directly: about 12 cm at the moment $t=12.5$ s after the beginning of the model seismic excitation, Fig. 15.

5. Discussion

5.1. Algorithm, boundary conditions, and tests

In the lithosphere part D_{lit} of the model medium, i.e. for simulation of the seismo-EM interaction, we applied: 1) the Galerkin approximation (e.g. Novik, 1995 where a theorem about the numerical stability was proved); 2) the explicit finite difference approximation of the hyperbolic equations of motion combined with the implicit approximation (the alternating direction method) of the parabolic equations of heat transfer and scalar magnetic potential (Novik and Ershov, 2001). We obtained the proper numerical

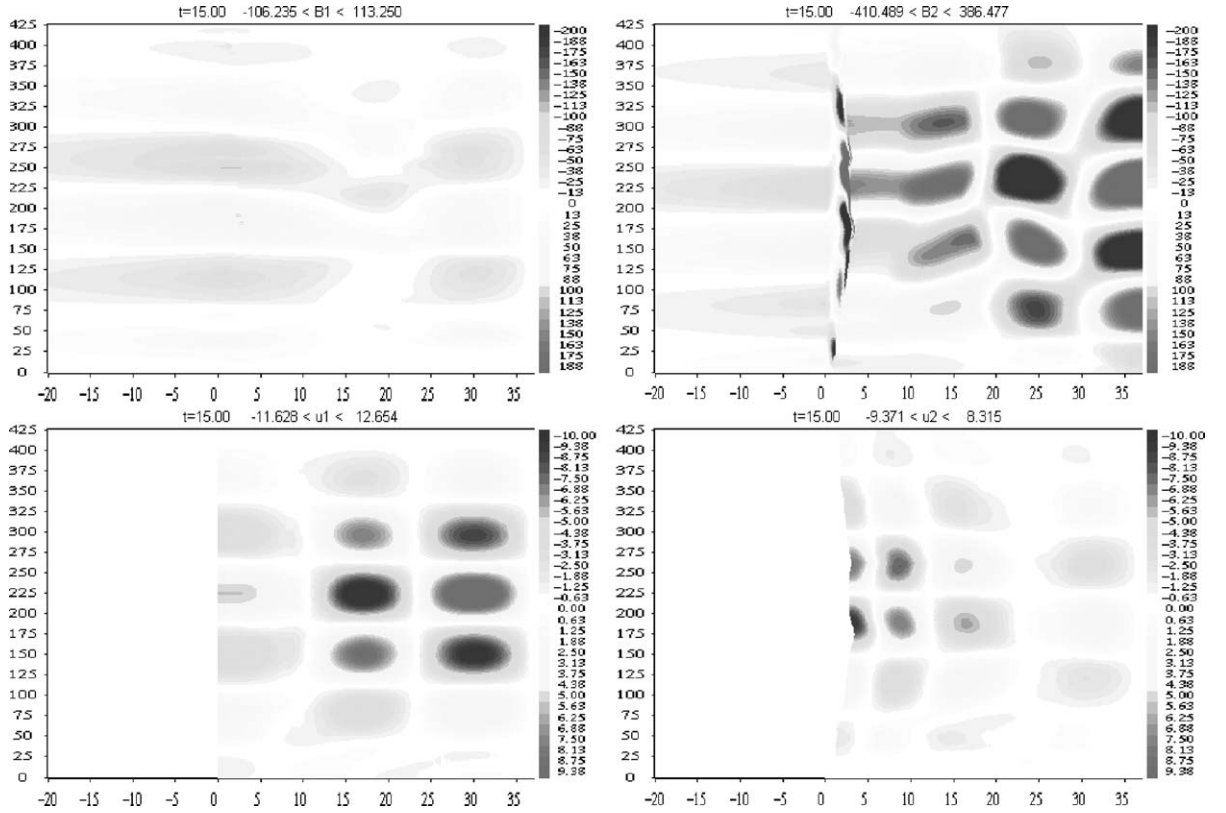

Fig. 10. The magnetic field diffusion trough the floor and surface of the sea filled up the rupture of the seismo-magnetic field. Peaks of the horizontal component of magnetic disturbance above the sea correspond to the spatial structure of the lithosphere seismic field replicated by the magnetic field under the sea (the lower right panel); S-wave is not propagating in the sea (low right panel), $t = 15.00$ s.

results by both methods, but the speed of the second one occurred to be higher by the same accuracy (below) and an acceptable size of memory. Hence the second method was used to calculate seismo-hydro-EM interaction in the lithosphere part of the lithosphere–hydrosphere–atmosphere domain according to model Eqs. (A.1)–(A.5). The hydrodynamic shallow water equations were rewritten in terms of the Riemannian invariants (e.g. Richtmyer, 1978) and directions of the characteristic lines were taken into account by the net approximation of the equations for the invariants and formulation of boundary

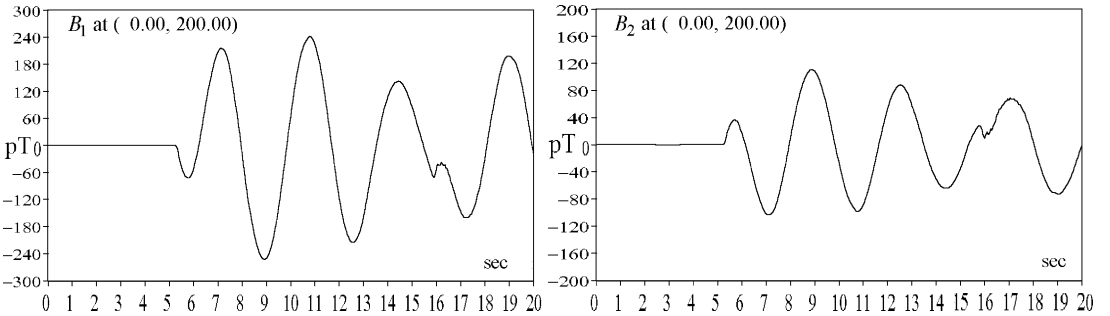

Fig. 11. The vertical (B_1) and horizontal (B_2) components of the seismic magnetic signal at the sea–atmosphere interface ($x = 0$) are represented by oscillations of the same low frequency range as the seismic excitation in the upper mantle under the sea (the horizontal co-ordinate $y = 200$ km).

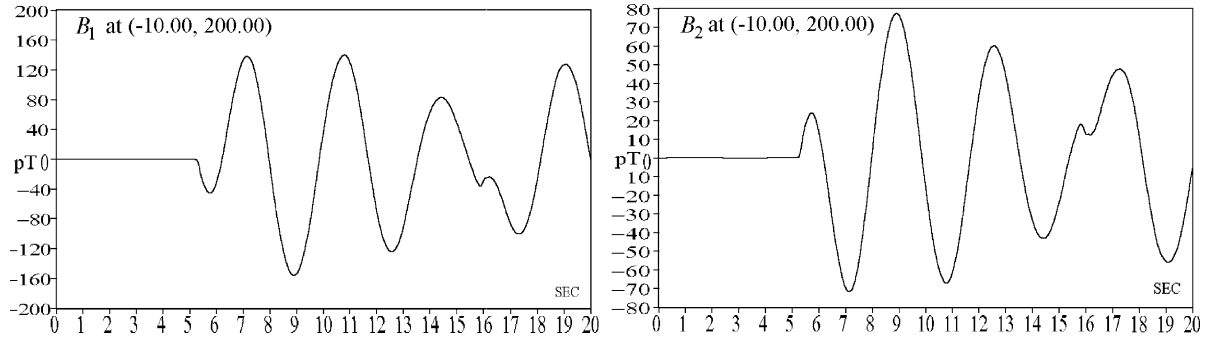

Fig. 12. The seismo-hydro-magnetic signal at the height of 10 km.

conditions. The co-ordinates and, correspondingly, the differential operators of field equations and boundary conditions, were transformed to get straight line as the lithosphere–hydrosphere boundary and to avoid a net approximation of the differential elasto-hydrodynamic contact conditions at a curvilinear boundary.

The same problem arises by the net approximation of the differential operators of the contact conditions at the boundaries of the lithosphere layers because of their active relief typical for seismic lithosphere zones. The space co-ordinate transformation allowing to get straight lines as the layers' boundaries for all layers simultaneously is possible but it is not reasonable from the computational point of view. As a well-known computational method for a piecewise homogenous medium D_{lit} we have applied the thin transition layers between main the ones determined by Fig. 1 and Table 1. If these auxiliary layers are thin enough (as compared with the size of D_{lit} at whole) and physical parameters' values change continuously in these layers then the dependence of the computed fields upon the thickness of the auxiliary layers (and upon the auxiliary medium parameters' values introduced in these layers) is negligible and the field values are practically the same (with an arbitrary accuracy) as by the field contact conditions at the boundaries of the main layers. Let us note, that it is a formulation (adopted for our case) of the theorem about stability of the solution of an initial boundary value problem against small (in the sense of an integral norm for D_{lit}) variations of the coefficients of differential equations. We should emphasize that though the thin transition layers exist between the homogenous (approximately) main layers in real geological structures, we have no proper data about them for the case of the Sea of Japan and the thin layers described above were introduced as a computational method only. Hence, these layers may not be included in the principal cross-section (Fig. 1). On the other hand, there were from 2 to 10 nodes along a vertical net line in the auxiliary layers, therefore, the thickness was of the order of a few hundreds of meters in different runs (see the net parameters below). So the auxiliary transition layers

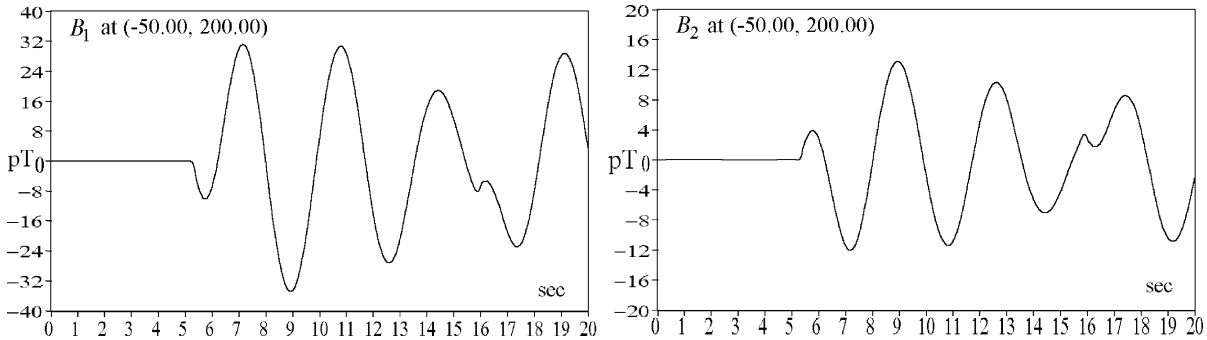

Fig. 13. The seismo-hydro-magnetic signal at the height of 50 km.

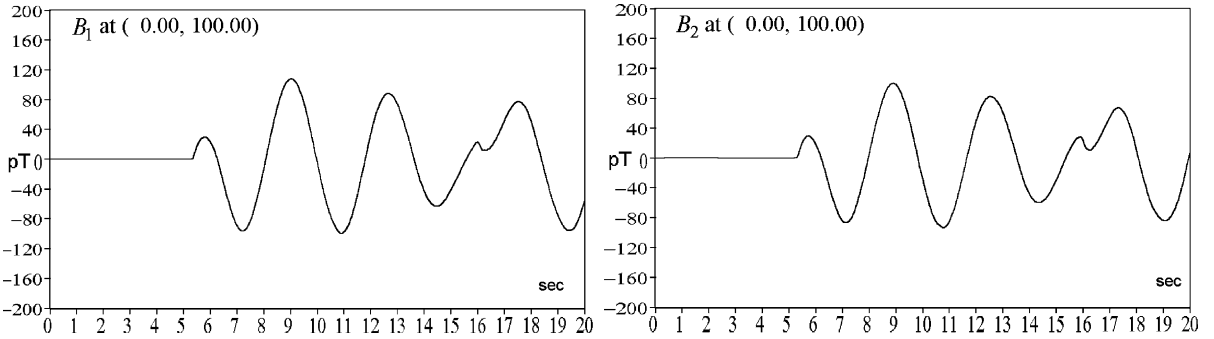

Fig. 14. The vertical (B_1) and horizontal (B_2) components of the seismic magnetic signal at the sea–atmosphere interface ($x=0$), horizontal co-ordinate $y=100$ km.

cannot be imaged by the vertical scale of Fig. 1. We checked that the computed field values are independent (with the accuracy of 10%) of thickness of the auxiliary transition layers. The dependence of the physical parameters of the medium upon the vertical co-ordinate was supposed to be linear in the transition layers (let us remember that any other continuous dependence is acceptable and the influence of this choice on the computed fields is negligible if the transition layers are thin enough as it is in our case). At the same time, at the sea surface we used contact condition (A.5) of continuity of the scalar potential and its derivative because this surface is almost plain (contrary to the boundaries of the lithosphere layers, Fig. 1) due to the small amplitude (Fig. 15) of the hydrodynamic long wave, as compared with the height (70 km) of the upper boundary of the atmosphere domain.

The magnetic permeability is supposed to be independent of spatial co-ordinates (see Section 2). Therefore the magnetic field components must becontinuous everywhere in the model medium including the lithosphere layers' contacts, sea bottom and sea surface. This condition, as one of the tests for the algorithm and program, was checked for the computed horizontal magnetic field component considered as the function of the vertical co-ordinate for a few fixed horizontal co-ordinates and moments of time, including ones after the seismic P wave shock into the sea bottom. In particular, we considered the subdomain near the sea bottom where the electric conductivity changes rapidly from small values in the sedimentary layer to large ones in seawater (Table 1). The discontinuities of the magnetic field components are absent there, as well as at the sea surface and other contacts.

The non-linear system of the net seismo-hydrodynamic contact conditions and hydrodynamic equations (in terms of the Riemannian invariants) was solved by iterations with controlled accuracy. To check this method, we constructed the method based on the system of integral equations deduced (using the Green function of the simplest heat transfer equation) from the shallow water equations with the 'vanishing viscosity' (Richtmyer, 1978). The evolution of a solitary hydrodynamic wave was described by two meth-

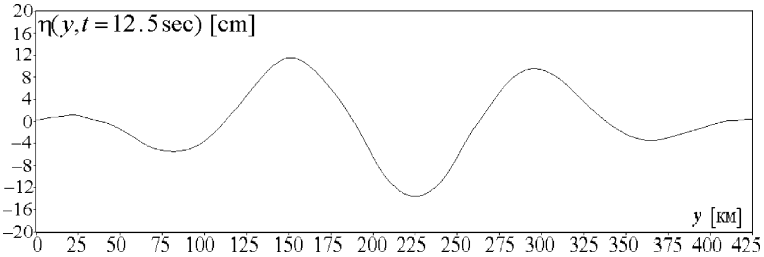

Fig. 15. The long seismo-hydrodynamic wave of a small amplitude far from a shore: η is the vertical co-ordinate of the sea surface, $t=12.50$ s after the beginning of the seismic excitation beneath the seafloor.

ods and the coincidence occurred to be satisfactory between these methods as well as with the well-known formula $(gh)^{1/2}$ for the velocity of the wave, where h is the depth of the water. Besides, steepness of the wave front was increasing in the course of moving to the shore.

Let us mention here, as an additional test, that our analysis of the magnetic field equation in seawater (with its high electric conductivity) on the basis of the incompressibility and contact conditions at the sea bottom and surface, showed: just after the seismic P wave's vertical shock into the sea bottom, a narrow domain of the vertical flow and a domain of negligible values of the horizontal component of magnetic induction arise in the sea interior along with the EM emission from its surface. In other words, Fig. 6 was deduced by us qualitatively from Eqs. (A.1)–(A.5) without computations (Ershov et al., 2001).

Numerical results were stable against a change of the mesh resolution. The difference between simulations with the spatial mesh resolution 500×500 by the time step of 0.005 s and 2000×2000 by the time step of 0.001 s was within 10%. Therefore the accuracy of computations is not less than the accuracy (about 20%) of geophysical and petrophysical data.

5.2. Comparison with observations

According to the tests above we believe that the numerical characteristics of the computed magnetic signals may not be distorted considerably (we mean the orders of magnitudes) by errors of the computational methods applied. So we are going to compare the computed co-seismic magnetic signal amplitude, delay in regard to the beginning of the model earthquake, and predominant frequency with the corresponding characteristics of observed co-seismic magnetic signals associated with earthquakes in the regions of the Sea of Japan and Kamchatka. Irrespective of the accuracy of computations, the orders of magnitudes may be compared only because of variety of the geophysical conditions of forming of the observed signals and lack of the data about these conditions (the physical and geometrical characteristics of geological structures along the traces of the seismic magnetic signals in the ocean lithosphere near Kamchatka and Japan, the spatial distribution of the salinity and seawater electric conductivity, the earthquake parameters, EM noises of different nature including the seafloor and other flows, the ionosphere disturbances and a high sea; see the end of Section 2 about stability of the computed signals' characteristics against the input data changes).

This paper is not a review (e.g. Johnston, 1997; Johnston and Parrot, 1998; Hayakawa and Molchanov, 2002; see also the references therein) of the co-seismic magnetic signals recorded in the near sea Pacific regions and only a few examples are described shortly in Table 2.

In this Table, the magnetic signal amplitude denotes the maximal value of magnetic induction for all components during the time interval of observation of a signal (about 10 to 30 s in the cases described here). In the 3rd row, the delay (22 s) of the seismic wave in regard to the magnetic signal was not described in the paper referenced in the last column, but we were known about this delay by Dr. Levshenko, V.T., see the paper (Gohberg et al., 1991). The delay (6 s) of the magnetic signal in regard to the earthquake beginning was obtained by us from the seismic and magnetic records published in the paper cited.

(Iyemori et al., 1996) detected the arrival of seismic wave 17 s after the beginning of the earthquake whereas the magnetic signal arrived without a visible delay (4th row of Table 2) but the error could be about 2 s by the time resolution available.

So, the magnitude of a co-seismic magnetic signal amplitude, according to the observation data cited in Table 2, is of the order of a few hundreds of pT at the sea level by an epicentral distance 50 to 100 km (and different earthquake magnitudes M_S), save for the case of 3rd row where the distance is twice as large.

In Section 4, the order of the magnitude of the computed magnetic signal amplitude is the same.

One can see from Table 2 that the typical delay of the recorded magnetic signals in regard to the earthquake beginning is about 5 s (taking account of a limited time accuracy of seismological investigations and the possible lag of magnetometers, (Belov et al., 1974)) and this signal parameter is practically independent of the epicentral distance.

These observations may be explained by the seismo-hydro-EM transformation mechanism visua-

Table 2
Parameters of co-seismic magnetic signals observed in regions of Kamchatka and Japan

No.	Date	M_S	Distance of the observation site from the epicentre (km)	Depth of the hypocentre (km)	Magnetic signal amplitude (pT)	Delay of the magnetic signal in regard to the earthquake beginning (s)	Delay of the seismic wave in regard to the magnetic signal (s)	Frequency interval or predominant frequency used to detect the signal (Hz)	Region of the observation site	Reference
1	11.10 1972	5	50	80	120	5	9	0.1–10	Petropavlovsk Kamchatsky, Russia	Belov et al., 1974
2	25.12 1972	6	70	70	430	4	10	0.1–10	Petropavlovsk Kamchatsky, Russia	Belov et al., 1974
3	01.09 1988	5.5	220	30	15	6	22	0.01–4	Kozyrevsk station, Kamchatka Russia	Gohberg et al., 1989
4	17.01 1995	7.2	100	17.2	600	0	17	1	Japan	Iyemori et al., 1996

lized in Section 3. Indeed, according to this mechanism, a delay of a magnetic signal depends mostly (see Section 5.3) on the time of propagation of a seismic P wave from a focal depth under a seafloor (37 km in our case) to the surface of the sea bottom, because the magnetic signal, after the seismic shock into the sea bottom surface, penetrates through the sea thickness immediately, along with the seismic disturbance of the incompressible (see (A.4)) water, and then the signal propagates with the light velocity above the sea. Therefore, as far as the delay of the magnetic signal in regard to the earthquake beginning is concerned, the epicentral distance is not of importance, according to mathematical model (A.1)–(A.5). Independence of a magnetic signal delay of an epicentral distance was obtained in our earlier computations of seismo-EM transformation for the case of the continental lithosphere (Novik et al., 1998; Novik and Ershov, 2001). From this point of view, the zero apparent delay of the magnetic signal in the last row of Table 2 may be explained by a relatively small hypocentral distance (17.2 km): the travel time of the seismic P wave from the hypocenter is from 2 to 3 s, i.e. it is just about the time accuracy (see above).

Let us remember, that the computed moment of the seismic P wave shock into the seafloor is $t_p=5.3$ s and the time of arrival of the magnetic signal at any point at the sea surface or above is the same (see the computed time series in Section 4; $t=0$ at the moment of the model earthquake beginning). So the computed magnetic signal delay corresponds to the observations.

The same is true for the computed magnetic signals' frequency ranges (see Section 4 and Figs. 11–14) and seismic wave's travel time (Fig. 6).

The computed electric (Novik et al., 2005), temperature and hydrodynamic seismo-disturbances' parameters correspond to the observations as well, but we omit an analysis similar to one performed above for the case of the computed magnetic signals (to reduce the volume of the paper).

5.3. Connection with other problems of the theory of sea bottom geothermal technologies

Any project of a sea bottom geothermal technology must provide for a monitored control sys-

tem to turn off, in a proper time, the prospecting, underwater drilling, pumping, power production, chemicals' extracting and transportation (vertical and horizontal) processes. It was clear from the very outset (Novik et al., 1998; see Section 1). But the December 26, 2004 geophysical catastrophe of the planetary scale sharpened drastically the problem of investigation and monitoring of the ocean lithosphere dynamics (Harinarayana and Hirata, in press).

Preliminary configuration of a monitoring system (see Section 6) based on the mathematical model (A.1)–(A.5) was described in (Novik et al., 2004, 2005). We hope, that similar seismo-hydro-EM lithosphere-Ocean-atmosphere monitoring systems will provide prognostic and warning information and also new data about the geophysical field interaction processes in tectonically active regions to develop the physical theory, mathematical models, computations, constructions and technologies for a wider class of dynamical geophysical conditions. For example, we recognize, that model Eqs.(A.1)–(A.5) must be expanded to take into account the compressibility of water and a limited (contrary to the incompressible case above) velocity of propagation of the acoustic and induced EM disturbances from the seismically deformed sea bottom to the sea surface. Our results (we hope to publish them) show that the delay of the computed magnetic signal in regard to the earthquake beginning should be increased in our case up to 7 s (in the deepest point of the sea) because the travel time of the hydro-acoustic wave must be added to the travel time of the seismic P wave.

Another theoretical problem is one of the seismic preparation processes' modeling for prognosis of a strong earthquake and magnetic location of the epicenter of a forthcoming earthquake (Kopytenko et al., 2002). Probably, the strengthening of the ULF activity (i.e. an increase in the amplitudes and a decrease in the gaps between pulses) observed by the authors of the referenced work (and by other researches) during the seismic preparation period is caused by intensification of the elementary acts of generating of EM signals resulting from the seismo-hydro-EM interaction described in Sections 3 and 4. Let us note that according to our calculations on the basis of model Eqs. (A.1)–(A.5), the amplitude of the computed signals increases along with the amplitude of a seismic excitation under a seafloor. Similar calculations should be used for prognostic interpretation of ULF signals.

Besides the geophysical problems (i.e. the main ones discussed in this paper), there are plenty of the important and difficult technological and economical problems of the operation of the sea bottom geothermal areas. For example, the expenditures, connected with: the lifting of the hot water from water bearing horizons to the sea bottom surface, its transportation (turbulent resistance) along the seafloor to the underwater stations, converting of heat energy and extracting chemical components, their transportation, transmitting of electric power and injection of the exhaust water into hydraulically isolated structures or other reservoirs (ecology), must be minimized under the following restrictions: the total volumes of the energy obtained and the chemical components extracted should be within the given limits during the given period of time; the outputs of every intake and its cone of depression (interference of intakes) should not exceed the prescribed values determined by the hydraulic pump characteristics (Novik and Mikhaylovskaya, 1998).

We underline here that a competitive prime cost may be obtained only as a result of an optimal control of technological processes. So the optimality criteria (e.g. the prime cost as a functional of the expenditures connected with the production and engineering development), restrictions and other problems of the theory of the sea bottom geothermal technology (practice of continental geothermal technologies should be used) must be investigated along with the theoretical and experimental geophysical problems of the sea bottom geothermal areas. The monitoring systems are not cheap and the expenditures may be returned partly by the sea technologies, including geothermal production. On the other hand, an underwater borehole with a negligible debit (may be, after some time of operation) can be used for the geophysical investigations of dynamical processes under the ocean bottom and prognosis, without influence of the factors of non-lithosphere origination.

6. Conclusion

On the basis of the nonlinear mathematical model of generation and propagation of seismo-EM signals in the basin of a marginal sea with an arbitrary 2D geological structure of the bottom (Section 2 and Appendix), we described numerically and graphically the transfer of seismic and EM energy from focal depths in the upper mantle to the sea (a rough schematization of the central part of the Sea of Japan) and EM emission from its surface into atmosphere up to heights near the lower boundary of the ionosphere.

*The computed signals' characteristics are of the same orders of magnitude (*Section 5*) as those observed*: the magnetic signal amplitude (a few hundreds of pT at the sea–air interface, Fig. 11), its main frequency (0.25 Hz); the delay of the computed seismic P wave in regard to the magnetic signal (about 20 s for receivers at the shore, it is clear from Figs. 1 and 6); the delay of the magnetic signal in regard to the beginning of a seismic excitation (about 5 s, the time of propagation in the air may be neglected, Section 3); the amplitude (12 cm), the length (about 150 km, Fig. 15) and the velocity of the hydrodynamic wave (a few hundreds of km/h far from the shore (Novik and Ershov, 2001)); the seismo-temperature disturbances at the top of the sedimentary layer (up to 0.02 K in different runs). Parameters of the signals recorded in the near sea seismic active regions, at the sea bottom and up to ionosphere may be found in e.g., (Belov et al., 1974; Gohberg et al., 1991; Hayakawa and Molchanov, 2002; Iyemori et al., 1996; Kopytenko et al., 2002; Di Mauro et al., 2002; Shpakovsky et al., 2002).

The simulated evolution of the spatial structure of the interacting fields as a whole (Figs. 3–10) may not be compared with a corresponding spatial-temporal picture derived from measurements. The described computed fields' evolution is based on:

- the main physical principles (i.e. on conservation laws of the theory of elasticity and hydrodynamics and on electrodynamics of slowly moving media);
- the assumptions about the lithosphere-hydrosphere-atmosphere medium and types of the processes considered (Sections 2 and 3);
- the mathematical investigations of algorithms (one of the typical theorems may be found in (Novik, 1995)).

A number of tests were done to verify our simulation programs against other algorithms or some analytic solutions; and a good agreement was shown.

We also realize that our simulation can be improved by making use of an advanced model of medium and its processes. However characteristics of time series of EM signals (i.e. characteristics comparable with measurements) are not expected to be significantly affected by the change to a better model because the simplest (one of our goals here) seismo-hydro-EM model already yields values close to that in natural observations.

Thus, according to the approach discussed, the magnetic recordings at the sea surface and above (buoys, balloons) should be combined with seismic, magnetic and temperature recordings at the sea bottom. The amplitudes of the expected precursory signals are: from tens of pT to 1 nT by frequencies from 0.01 to 10 Hz for seismo-magnetic signals and from 0.001 to 1 K for seismo-temperature ones (quartz thermo-resistors should be applied). Details may be found in (Di Mauro et al., 2002; Kopytenko et al., 2002; Novik et al., 2004, 2005; Romanowicz et al., 2001).

Acknowledgments

We are grateful to Profs. N.S. Erokhin, G.G. Malinetsky, Yu. Ya. Ruzhin, V.S. Shneyer, and Ramesh P. Singh for valuable discussions; thanks are also due to Dr. D.G. Repin for the geophysical data. We thank the reviewers and the editors for the remarks.

Appendix A. Field equations

According to the principles of the theory of magnetothermoelasticity (Maugin, 1988), under our

assumptions on medium and field dynamics (see Section 2) the evolution of fields in the lithosphere part D_{lit} of the medium obeys

$$\rho\frac{\partial^2 u_i}{\partial t^2}=\frac{\partial}{\partial x_k}\left(\mu\left(\frac{\partial u_i}{\partial x_k}+\frac{\partial u_k}{\partial x_i}\right)\right)+\frac{\partial}{\partial x_i}\left(\lambda\frac{\partial u_k}{\partial x_k}\right)-\frac{\partial(\beta\theta)}{\partial x_i}+\rho g_i,\quad i=1,2\quad \frac{\partial A}{\partial t}=\frac{1}{\mu_0\sigma_e}\Delta A-v_k\frac{\partial A}{\partial x_k}+v_2H_{1,0}-v_1H_{2,0}\quad \rho c_V\frac{\partial\theta}{\partial t}=\frac{\partial}{\partial x_k}\left(\kappa\frac{\partial\theta}{\partial x_k}\right)-\beta\theta_0\frac{\partial v_k}{\partial x_k}+\frac{1}{\sigma_e}(\Delta A)^2+q. \tag{A.1}$$

Here and below we assume summation over repeated indices $i,j,k=1,2$.

Notations are: $\boldsymbol{u}=(u_1(t,\boldsymbol{x}),\ u_2(t,\boldsymbol{x}))$ is the elastic displacement at the point $\boldsymbol{x}\in D_{\mathrm{lit}}$, $\boldsymbol{x}=(x_1,x_2)$, at the moment t (in previous sections: $\boldsymbol{x}=(x,y)$); g_1 is the acceleration of gravity and $g_2=0$; $\mu(\boldsymbol{x})$ and $\lambda(\boldsymbol{x})$ are the elastic parameters of Lame, $\beta=(2\mu+3\lambda)\alpha$ where $\alpha(\boldsymbol{x})$ is the coefficient of thermal expansion; $A(t,\boldsymbol{x})$ is the scalar seismo-magnetic potential existing for 2D media with uniform magnetic permeability such that the seismic disturbance of the magnetic field intensity is $H_1=-\partial A/\partial x_2$, $H_2=\partial A/\partial x_1$, while $H_{1,0}$ and $H_{2,0}$ is the intensity of the stationary geomagnetic field which is supposed to be uniform (existed prior to seismic perturbation); $\boldsymbol{v}=(v_1,v_2)=\partial\boldsymbol{u}/\partial t$ is velocity; and $\vartheta(t,x)=\Theta(t,\boldsymbol{x})-\vartheta_0$ is the deviation of temperature Θ from its initial value ϑ_0 existed at $t=0$; q is the density of the power of heat sources (see Section 2 and Table 1).

At the sea bottom the normal component v_{n} of the elastic velocity $\boldsymbol{v}$ equals the normal component w_{n} of the water velocity $\boldsymbol{w}$; the normal component of the force acting from the sediment layer equals the water pressure p, while the tangent component of this force vanishes because we neglect shear stresses in water. Neglecting compressibility and viscosity of the sea water, non-hydrostatic component of pressure and heat transfer, we can describe the water dynamics in the framework of the "shallow water" theory, (e.g. Stoker, 1957) which operates horizontal velocity w_2 (in this approximation it is independent of the depth x_1) and elevation of sea surface $\eta(t,x_2)$:

$$\frac{\partial}{\partial t}(\eta+h)+\frac{\partial}{\partial x_2}((\eta+h)w_2)=0,\qquad \frac{\partial w_2}{\partial t}+w_2\frac{\partial w_2}{\partial x_2}+g\frac{\partial\eta}{\partial x_2}=0 \tag{A.2}$$

where $h=h(t,x_2)$ is the vertical co-ordinate of the sea bottom surface which is moving according to the seismic deformation process.

The magnetic potential A in the water obeys the same equation as in elastic medium, save for the elastic velocity field $\boldsymbol{v}$ replaced by the water velocity $\boldsymbol{w}=(w_1,\ w_2)$:

$$\frac{\partial A}{\partial t}=\frac{1}{\mu_0\sigma_e}\Delta A-w_k\frac{\partial A}{\partial x_k}+w_2H_{1,0}-w_1H_{2,0}. \tag{A.3}$$

The component w_1 is calculated using the hydroelastic conjugation condition (above) and the incompressibility condition

$$\frac{\partial w_1}{\partial w_2}+\frac{\partial w_2}{\partial x_2}=0. \tag{A.4}$$

We assume that electric conductivity is continuous across the sea bottom (due to percolation of seawater) and the conjugation conditions for A are not needed at the sea bottom, whereas the conjugation condition at the sea surface $x_1=0$ is as follows: A and its normal derivative are continuous across the sea surface; in the atmosphere $A(t,\boldsymbol{x})$ satisfies the Laplace equation which is the limit of the magnetic diffusion equation for vanishing electric conductivity of the air:

$$\Delta A=0,\quad x_1<0,\ 0<x_2<L_2,\ t>0;\qquad A(t,+0,x_2)=A(t,-0,x_2),\qquad \left.\frac{\partial A}{\partial x_1}\right|_{x_1=+0}=\left.\frac{\partial A}{\partial x_1}\right|_{x_1=-0}. \tag{A.5}$$

This equation is stationary, but the electromagnetic field conjugation conditions at the sea surface depend on the non-stationary electromagnetic process in the sea controlled by seismo-hydrodynamic flow resulting from seismic deformation of the sea bottom.

The *initial conditions* were chosen so that before the moment $t=0$ the model medium was at rest, thus

the water velocities and the elevation of sea surface is 0; the configuration of the elastic displacement field is stationary under the gravity force; the initial magnetic field is uniform in space: $H_{1,0}=30$, $H_{2,0}=35$ [A/m]. For all of the fields in the computations described above, the normal derivative vanishes at the left ($x_2=0$) and right ($x_2=L_2$) boundaries, for the magnetic potential this derivative vanishes at the boundaries $x_1=L_1$ and $x_1=-L_D$ as well. The temperature disturbance is supposed to be zero at the sea bottom surface whereas the seismic disturbance of the heat flow is zero at the lower boundary of the model medium.

Therefore, the model seismic excitation arising at the moment $t=0$ at the lower boundary of the lithosphere-Ocean-atmosphere medium, i.e. the non-stationary boundary value condition for the elastic field (Section 2), is the only factor disturbing the rest of this model medium and turning on the non-stationary seismo-hydro-EM interaction and signals' generation including the magnetic ones.

So, the geophysical field interaction model is represented in the lithosphere by the system of partial differential equations including hyperbolic (dynamic theory of elasticity) and parabolic (magnetic diffusion and heat transfer) operators; the structure of the interaction model in the sea is the same with the hyperbolic operator of the theory of elasticity replaced by the hyperbolic operator of the "shallow water" theory. Mathematical results regarding systems of partial differential equations with coupled hyperbolic and parabolic operators may be found in (Novik, 1995; Novik and Ershov, 2001) and other publications of the authors.

We obtained the proper results by using the Galerkin and finite-difference methods for the computation of the lithosphere fields' evolution and by other tests (e.g. the control of the accuracy of the hydrodynamic component of the solution and the hydro-elastic contact conditions, see Section 5 for other details).

References

Arora, B.R., Mahashabde, M.V., 1987. A transverse conductive structure in the Northwest Hymalaya. Physics of the Earth and Planetary Interiors 45, 119–127.

Belov, S.B., Migunov, N.I., Sobolev, S.A., 1974. Magnetic effects accompanying strong earthquakes at Kamchatka. Magnetism i Aeronomya (Magnetism and Aeronomy) 14, 380–382 (in Russian).

Biagi, P.F., Kingsley, S.P., Parrot, M. (Eds.), Earthquake Precursors, Physics and Chemistry of the Earth, vol. 23, pp. 909–973.

Bragin, V.D., Volykhin, A.M., Trapesnikov, Yu.A., Koshin, N.A., Batalev, V.Yu., 1993. Depth structure of seismicity-dangerous zones of the Tang Shan based on electromagnetic sounding data. Journal of Earthquake Prediction Research 2, 329–338.

Di Mauro, D., De Santis, A., Palangio, P., Romeo, G., D'Anna, G., D'Anna, R., Favali, P., 2002. Consideration on the magnetic recordings from southern Tyrrhenian Sea bottom (Geostar experiment). Book of Abstracts of III International Workshop on Magnetic, Electric and Electromagnetic Methods in Seismology and Volcanology (MEEMSV-2002), Moscow.

Ershov, S.V., Mikhaylovskaya, I.B., Novik, O.B., 2001. Electromagnetic (EM) signals of seismic excitation of geological structures beneath a sea bottom. Physics and Chemistry of the Earth 26, 761–768.

Gohberg, M.B., Krylov, S.M., Levshenko, V.T., 1991. The electromagnetic field of the earthquake focus. Transactions (Doklady) of the Russian Academy of Sciences, Geophysics 308, 1–3 (Translated from Russian: Doklady Akademii Nauk USSR, 1989, vol. 308, No 1, pp. 62–65).

Harinarayana, T., Hirata, N., in press. Distractive Earthquake and Disastrous Tsunami in the Indian Ocean, What Next? Gondwana Research (Gondwana Newsletter Section, International Association for Gondwana Research, Japan), 8 (2).

Hayakawa, M., Molchanov, O. (Eds.), 2002. Seismo-Electromagnetics. Terra Scientific Publishing Company, Tokyo.

Hellweg, K.-H. (Editor in Chief), 1982. Numerical data and Functional Relationships in Science and Technology. New Series. Group V: Geophysics and Space Research, Vol. I, Physical Properties of Rocks, Subvolume B (Editor: Angenheister, H.), Springer.

Honkura, Y., 1974. Electrical conductivity anomalies beneath the Japan Arc. Journal of Geomagnetism and Geoelectricity 26, 147–171.

Johnston, M.J.S., 1997. Review of electric and magnetic fields accompanying seismic and volcanic activity. Surveys in Geophysics 18, 441–475.

Johnston, M.J.S, Parrot, M. (Eds.), 1998. Physics of the Earth and Planetary Interiors, vol. 105, pp. 3–4.

Iyemori, T., Kamei, T., Tanaka, Y., Takeda, M., Hashimoto, T., Araki, T., Okamoto, T., Watanabe, K., Simitomo, N., Oshima, N., 1996. Co-seismic geomagnetic variations observed at the 1995 Hyogoken-Nanbu earthquake. Journal of Geomagnetism and Geoelectricity 48, 1059–1070.

Kopytenko, Yu, Imagilov,, Hattori, K., Voronov, P., Hayakawa, M., Molchanov, O., Kopytenko, E., Zaitsev, D., 2002. Monitoring of the ULF electromagnetic disturbances at the station network before EQ in seismic zones of Izu and Chiba Peninsulas (Japan). In: Hayakawa, M., Molchanov, O. (Eds.), Seismoelectromagnetics: Lithosphere-Atmosphere-Ionosphere Coupling. Terra Scientific Publishing Company, Tokyo.

Maugin, G.A., 1988. Continuum Mechanics of Electromagnetic Solids. North-Holland, Amsterdam.

McDuff, R.E., 1995. Physical dynamics of deep-sea hydrothermal plumes. Seafloor Hydrothermal Systems, Physical, Chemical, Biological, and Geological Interactions, Geophysical Monograph, vol. 91. American Geophysical Union.

Novik, O.B., 1995. The Galerkin method for a three-dimensional nonlinear system of magneto-thermoelasticity equations. Transactions (Doklady) of the Russian Academy of Sciences. Earth Science Sections 335A (3), 15–21 (Translated from Russian: Doklady Rossiyskoy Akademii Nauk, 334, 100–102, 1994).

Novik, O.B., Ershov, S.V., 2001. Electromagnetic and Temperature Signals from the Earth's Depth (Scientific Monographs of Federal Program of Integration of High Education and Fundamental Science Moscow, in Russian).

Novik, O.B., Mikhaylovskaya, I.B., 1998. Optimal outputs of thermal water intakes. Proceedings of the International Conference on The Earth Thermal Field and Related Research Methods. Moscow State Geological Surveying Institute.

Novik, O.B., Ershov, S.V., Mikhaylovskaya, I.B., 1998. Mathematical problems of seismological monitoring of geothermal areas. Proceedings of the XXIII Workshop on Geothermal Reservoir Engineering. Stanford University.

Novik, O.B., Ershov, S.V., Mikhaylovskaya, I.B., 2000a. Mathematical model of tsunamis' electromagnetic signals. Book of Abstracts, 2000 Fall Meeting. American Geophysical Union.

Novik, O.B., Ershov, S.V., Mikhaylovskaya, I.B., Repin, D.G., 2000b. Geothermal areas at a sea bottom: geophysics. Proceedings of XXIII Workshop on Geothermal Reservoir Engineering. Stanford University.

Novik, O.B., Ershov, S.V., Mikhaylovskaya, I.B., 2001. Electromagnetic signals in atmosphere caused by dynamic processes in ocean lithosphere. Proceedings of the 15th European Space Agency Symposium on Rocket and Balloon Programs and Related Research. Biarritz, France.

Novik, O.B., Ershov, S.V., Mikhaylovskaya, I.B., Ruzhin, Yu. Ya., 2004. Theory of electromagnetic tsunami precursors. Mode Conversion, Coherent Structures and Turbulence, Proceeding of International Conference. Space Research Institute of Russian Academy of Sciences.

Novik, O., Ruzhin, Yu., Ershov, S., 2005. EM Tsunami monitoring: theory and recommendations. In: Satake, K. (Ed.), Tsunamis: Case Studies and Recent Developments. Springer, pp. 319–340.

Richtmyer, R.D., 1978. Principles of Advanced Mathematical Physics, vol. 1. Springer-Verlag, New York, Heidelberg, Berlin.

Romanowicz, B., Suyehiro, K. Kawakatsu, H., (Eds), 2001. Long-Term Observations in the Oceans, Ocean Hemisphere Project and International Ocean Network (OHP/ION), Joint Symposium, Workshop Report, Japan.

Shpakovsky, V., Ruzhin, Yu. Ya., Kanonidi, Kh. D., Osipov, N.K., 2002. Regional ionosphere behavior and SQ-variations as earthquake precursors for Kamchatka area. Book of Abstracts of the World Space Congress—2002. Committee on Space Research.

Stoker, J.J., 1957. Water Waves. Interscience Publishers Inc., New York.